References and Notes

1. C. F. Yoder *et al.*, *Nature* **303** 757 (1983).
2. D. P. Rubincam, *J. Geophys. Res.* **89**, 1077 (1984).
3. M. K. Cheng, C. K. Shum, B. D. Tapley, *J. Geophys. Res.* **102**, 22377 (1997).
4. C. M. Cox, S. M. Klosko, B. F. Chao, in *Gravity, Geoid and Geodynamics 2000: International Association of Geodesy Symposium*, M. Sideris, Ed. (Springer-Verlag, Heidelberg, Germany, 2002), vol. 123, pp. 355–360.
5. F. G. Lemoine *et al.*, *NASA Technical Publication 206861* (NASA Goddard Space Flight Center, Greenbelt, MD, 1998).
6. These weights correspond to a data uncertainty of about 1 to 2 m for the SLR data (*4*), which is 10 to 20 times larger than the data performance. This is representative of the uncertainties generally derived in gravity model development (*5*) and appears to be the result of limitations in the forward modeling and solution parameterization.
7. R. S. Nerem *et al.*, *Geophys. Res. Lett.* **27**, 1783 (2000).
8. B. F. Chao, W. P. O'Connor, *Geophys. J.* **94**, 263 (1988).
9. B. F. Chao, A. Y. Au, *J. Geophys. Res.* **96**, 6577 (1991).
10. A. Cazenave *et al.*, *Earth Planet. Sci. Lett.* **171** 549 (1999).
11. Data from the National Center for Environmental Prediction, National Oceanic and Atmospheric Administration, are available at http://wesley.wwb.noaa.gov/cdas_data.html.
12. The IB is a correction for a fluid-loading effect that assumes that the ocean surface height responds isostatically to overlying atmospheric pressure. It is most accurate at large spatial scales and time periods longer than weeks, which are applicable to this analysis. For reference see C. Wunsch, D. Stammer, *Rev. Earth Planet. Sci.* **26**, 219 (1998).
13. J. X. Mitrovica, W. R. Peltier, *J. Geophys. Res.* **98**, 4509 (1993).
14. D. Han, J. Wahr, *Geophys. J. Int.* **120**, 287 (1995).
15. T. S. James, E. R. Ivins, *J. Geophys. Res.* **102**, 605 (1997).
16. B. F. Chao, *Geophys. Res. Lett.* **22**, 3529 (1995).
17. National Research Council, *Abrupt Climate Change*, R. Alley, Ed. (National Academy Press, Washington, DC, 2001). This comprehensive report calls attention to modern findings regarding past abrupt climate changes, the most notable of which occurred over periods of just a few years.
18. W. Krabill *et al.*, *Science* **289**, 428 (2000).
19. Results were provided by J. Zwally (Goddard Space Flight Center), using techniques described by J. Zwally, A. Brenner, in *Altimetry and Earth Science*, L. L. Fu, A. Cazenave, Eds. (Academic Press, London, 2001) pp. 351–369.
20. For example, see A. A. Arendt, K. A. Echelmeyer, W. D. Harrison, C. S. Lingle, V. B. Valentine, *Science* **297**, 382 (2002).
21. M. Dyurgerov, M. Meier, *Proc. Natl. Acad. Sci. U.S.A.* **97**, 1406 (2000).
22. The modern GSL rise is estimated to be 1.5 to 2 mm/year [B. Douglas, M. Kearney, S. Leatherman, Eds., *Sea Level Rise* (Academic Press, San Diego, CA, 2001)]. It is due to the steric (thermal plus salinity) effect plus the water mass addition.
23. Results were provided by the NASA Ocean Altimeter Pathfinder Project and are available at http://iliad.gsfc.nasa.gov/ocean.html.
24. S. Levitus, J. I. Antonov, T. P. Boyer, C. Stephens, *Science* **287**, 2225 (2000).
25. C. Cabanes, A. Cazenave, C. Le Provost, *Science* **294**, 840 (2001).
26. M. Alexandrescu, D. Gilbert, G. Hulot, J. L. Le Mouël, G. Saracco, *J. Geophys. Res.* **101**, 21975 (1996).
27. M. Mandea, E. Bellanger, J. L. Le Mouël, *Earth Planet. Sci. Lett.* **183**, 369 (2000).
28. Results provided by W. Kuang (University of Maryland Joint Center for Earth Technology), based on models described in W. Kuang, J. Bloxham, in *The Core-Mantle Boundary Region*, M. Gurnis *et al.*, Eds. (AGU, Washington, DC, 1998) pp. 197–208.
29. L. L. Fu, R. D. Smith, *Bull. Am. Meteorol. Soc.* **77**, 2625 (1996).
30. D. R. Stammer *et al.*, *J. Geophys. Res.* **101**, 25779 (1996).
31. T. J. Johnson, C. R. Wilson, B. F. Chao, *J. Geophys. Res.* **106**, 11315 (2001).

32. We thank A. Au and J. Beall of Raytheon ITSS for their data-processing assistance. We have benefited from discussions with M. Cheng, R. Eanes, S. Klosko, S. Nerem, E. Ivins, W. Kuang, M. Purucker, and V. Zlotnicki. Supported by NASA's Oceanography Program and Solid Earth and Natural Hazards Program. The SENH program also supports NASA's SLR network.

Supporting Online Material

www.sciencemag.org/cgi/content/full/297/5582/831/DC1

Figs. S1 to S4

25 March 2002; accepted 14 June 2002

Foraminiferal Calcification Response to Glacial-Interglacial Changes in Atmospheric CO_2

Stephen Barker* and Henry Elderfield

A record of foraminiferal shell weight across glacial-interglacial Termination I shows a response related to seawater carbonate ion concentration and allows reconstruction of a record of carbon dioxide in surface seawater that matches the atmospheric record. The results support suggestions that higher atmospheric carbon dioxide directly affects marine calcification, an effect that may be of global importance to past and future changes in atmospheric CO_2. The process provides negative feedback to the influence of marine calcification on atmospheric carbon dioxide and is of practical importance to the application of paleoceanographic proxies.

Higher concentrations of carbon dioxide in the atmosphere cause surface seawater to become more acidic and lower the calcium carbonate saturation state through the consequent decrease in $[CO_3^{2-}]$, the carbonate ion concentration (*1*). Predictions suggest that the carbonate saturation state will be reduced by 30% relative to the preindustrial level by the middle of the 21st century (*1*, *2*). This has raised concern because of evidence that carbonate saturation is correlated with the rate of production of marine calcium carbonate and because of studies showing that coral reefs and some species of coccolithophorids (major producers of marine carbonate) are sensitive to elevated CO_2 pressure (PCO_2) (*3*–*7*). The hypothesis that growth rate is a function of $[CO_3^{2-}]$ is also consistent with inorganic studies (*8*, *9*).

If marine calcification is sensitive to the concentration of atmospheric carbon dioxide, its effect should be reflected in the paleoceanographic record as a response to glacial-interglacial fluctuations in PCO_2. Foraminifera constitute an important fraction of marine plankton and play a significant role in the carbon cycle through the production of shell calcite. Increased carbonate ion concentrations in culturing experiments using the planktonic foraminifer *Orbulina universa* have been shown to produce higher shell weights in similarly sized organisms, interpreted as a consequence of thicker shell walls resulting from higher rates of calcification (*10*, *11*). We have found that shell weights of several species of planktonic foraminifera from core top sediments vary systematically as a function of latitude in the North Atlantic. By combining these findings with a record of shell weight across glacial-interglacial Termination I, we demonstrate that the changes are as a result of ambient $[CO_3^{2-}]$ changes rather than calcification temperature and are consistent with known changes in atmospheric PCO_2. The link between marine calcification and $[CO_3^{2-}]$ provides a negative feedback to changes in atmospheric PCO_2. This observation is also of practical importance in paleoceanography because shell weight is used as an index of carbonate dissolution at the seafloor and, thus, of past changes in deep-sea $[CO_3^{2-}]$ (*12*).

Measured weights of several planktonic foraminiferal species (picked from narrow size fractions) from a North Atlantic latitudinal transect (*13*) increase by a factor of about 2 between 60° and 30°N (Fig. 1A). Due to the strong temperature dependence of CO_2 solubility in seawater, and the subsequent dissociation of $CO_{2(aq)}$ into HCO_3^- and CO_3^{2-}, modern open ocean surface water $[CO_3^{2-}]$ varies as a function of temperature. Thus, the observed trend in shell weight would fit with a $[CO_3^{2-}]$ control as well as a temperature control. An offset in the shell weights of *Pulleniatina obliquiloculata* and *Neogloboquadrina dutertrei* has been reported between the tropical Atlantic, Indian, and Pacific

Department of Earth Sciences, University of Cambridge, Cambridge CB2 3EQ, UK.

*To whom correspondence should be addressed. E-mail: sbar98@esc.cam.ac.uk

Ocean basins, but no such offset is found for the shallower dwelling *Globigerinoides sacculifer* (*12*). The similarity in surface ocean temperature profiles between these ocean basins seems to negate a temperature control on shell weight. However, $[CO_3^{2-}]$-temperature relations are not constant from basin to basin and, as a result, varying offsets in $[CO_3^{2-}]$ occur at different depths between the oceans. These offsets may be sufficient to explain the anomalous offsets in shell weight.

Various approaches could be made to test the relation between $[CO_3^{2-}]$ and shell weight. It has suggested that a comparison of modern foraminiferal tests taken from the water column with those from core tops would discriminate between a temperature control and a carbonate ion control (*14*). If the control is carbonate ion, foraminifera from the water column should weigh less than those from core tops, reflecting the decrease in surface ocean $[CO_3^{2-}]$ resulting from atmospheric PCO_2 increase since preindustrial times, whereas a temperature control would produce a change in the opposite direction. An alternative yet analogous approach, which we have adopted, is to chart the evolution of shell weight through time. We analyzed the shell weights of *Globigerina bulloides* through Termination I in a shallow sediment core from the North Atlantic (NEAP 8K, collected as part of the North East Atlantic Palaeoceanography and Climate Change (NEAPACC) project, 59°48'N 23°54'W; water depth, 2360 m). Results were combined with paleotemperature (via Mg/Ca thermometry) and salinity records from the same core in order to constrain the major parameters associated with the ocean carbonate system. Atmospheric PCO_2 at the last glacial maximum (LGM) was ~90 ppmV lower than preindustrial (Holocene) values (thus, surface ocean $[CO_3^{2-}]$ was higher) and temperature was lower as well. Therefore, a temperature control would be indicated by lower shell weights before Termination I, whereas a carbonate ion control would be indicated by higher shell weights.

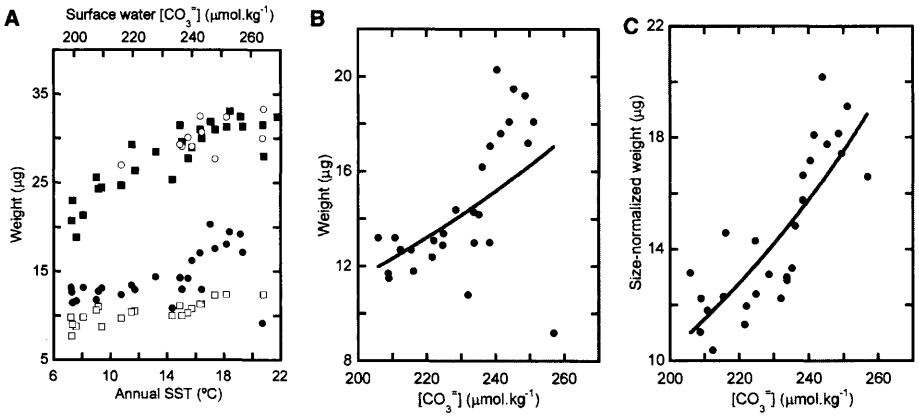

Fig. 1. (**A**) Shell weights of four species of planktonic foraminifera from the North Atlantic between 60° and 30°N latitude plotted against modern sea surface temperature (SST) at the core sites (*28*). Also shown are corresponding values of surface water $[CO_3^{2-}]$ (based on the linear relation between temperature and $[CO_3^{2-}]$) corrected to preindustrial values (*20*). Solid circles, *Globorotalia bulloides* (300 to 355 µm); open circles, *Globorotalia truncatulinoides* (300 to 355 µm); solid squares, *Globorotalia inflata* (300 to 355 µm); open squares, *Neogloboquadrina pachyderma* (dextral) (250 to 300 µm). (**B**) Shell weight and (**C**) size-normalized shell weight for *G. bulloides* plotted against preindustrial $[CO_3^{2-}]$ (*20*). Heavy lines in (B) and (C) represent best-fit exponential curves to the data.

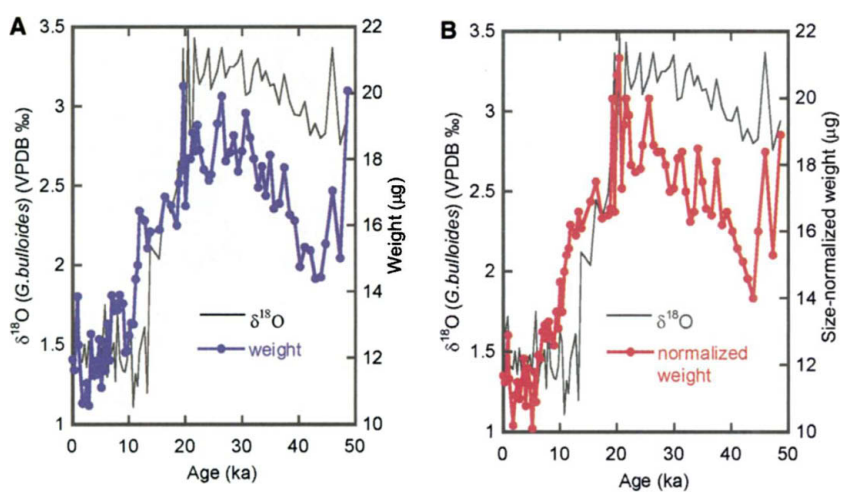

Fig. 2. (**A**) Measured shell weight and (**B**) size-normalized shell for *G. bulloides* plotted with $\delta^{18}O$ [data from (*32*)] for the same species in NEAP 8K [age model from (*33*)].

Down-core records of shell weight and size-normalized shell weight (*15*) for *G. bulloides* are plotted with the $\delta^{18}O$ record of *G. bulloides* from the same core (Fig. 2). Shell weights are highest during the LGM and show a large decrease into the early Holocene. This trend is also recognizable in other, lower resolution, records used to study carbonate dissolution in the Atlantic Ocean (*16*, *17*). The fact that shell weights are heavier during glacial times suggests that the control on shell weight is carbonate ion and not calcification temperature. A potential complication is that, alternatively, the control is higher carbonate preservation in the glacial samples.

NEAP 8K is situated well above the modern-day lysocline in the NE Atlantic Ocean and is bathed in high-$\delta^{13}C$, low-nutrient North Atlantic deep water (NADW). During the LGM, the site lay at the transition between similarly high-$\delta^{13}C$ glacial North Atlantic intermediate water (GNAIW) and low-$\delta^{13}C$ Antarctic bottom water (AABW) (*18*, *19*). The increased influence of low-$\delta^{13}C$, nutrient-rich waters at the site of NEAP 8K would probably have caused a lowering of bottom water carbonate saturation and a decrease in preservation potential of carbonate sediments. Therefore, we should expect to see lighter glacial shell weights in NEAP 8K if dissolution was a major control on shell weight at this site. The observed increase in glacial shell weight suggests that this is not a preservation signal.

To evaluate quantitatively whether the record through Termination I can be ascribed to a carbonate ion effect, we first used the data from the core-top transect to establish the relation between $[CO_3^{2-}]$ and foraminiferal shell weight and then go on to estimate surface-ocean paleo-PCO_2. Shell weight (Fig. 1B) and size-normalized weight data (Fig. 1C) for *G. bulloides* are plotted against preindustrial $[CO_3^{2-}]_{surface(50m)}$ (*20*). Adjustment to preindustrial values is necessary for the calibration as the average age of core-top samples is >200 years, since when surface-ocean $[CO_3^{2-}]$ has decreased as atmospheric PCO_2 increased. Comparison of the plots highlights the benefit of correcting weight data for size variations. Samples with considerably lower weights than would be predicted from the overall trend (Fig. 1B) are those with a mean shell size that is lower than average. Recognizing the uncertainties implicit from the scatter in the correlation (of course, the ages of the core tops vary and, hence, our assumption of a constant offset

between modern and preindustrial [CO_3^{2-}] is not strictly correct), this calibration is used to interpret the down-core size-normalized weight record from NEAP 8K in terms of [CO_3^{2-}] (Fig. 3A). The antiphase relation between the records of calculated [CO_3^{2-}] and atmospheric CO_2 from the Vostok ice core (*21*) supports the hypothesis that foraminiferal shell weight is related to a component of the ocean-atmosphere carbonate system.

The relation between atmospheric PCO_2 and the carbonate species within surface waters can be described to a first approximation by the thermodynamic relations

$$CO_2(g) \overset{K_0}{=} CO_2(aq) + H_2O \overset{K_1}{=} HCO_3^- + H^+ \overset{K_2}{=} CO_3^{2-} + 2H^+$$

which lead to

$$PCO_2 = (0.96[TA] - 2[CO_3^{2-}])^2 / [CO_3^{2-}]K'$$

where K_0 is the solubility coefficient of CO_2 in seawater, K_1 and K_2 are the first and second dissociation constants of carbonic acid [functions of temperature (T) and salinity (S)], K' is K_0K_1/K_2, and TA is the total alkalinity (*22*). Accordingly, knowledge of [CO_3^{2-}], T, S, and TA, will allow approximate calculation of PCO_2. Temperature and salinity were estimated by combining Mg/Ca thermometry with $\delta^{18}O$ data on the same foraminiferal samples (Fig. 4) (*23*). Although TA is a linear function of salinity in the modern surface ocean, it is not clear whether this relation is constant through time. Therefore, estimates were made for different values of TA (*23*).

The record of surface-ocean PCO_2 ($PCO_{2(aq)}$) for NEAP 8K obtained in this manner displays a trend similar to that observed for atmospheric CO_2 as recorded in Antarctic ice (Fig. 3B). The glacial to interglacial increase in $PCO_{2(aq)}$ of around 80 to 90 ppm agrees with estimates from ice records. In general, $PCO_{2(aq)}$ values are about 40 ppm lower than atmospheric CO_2 concentrations. This is in line with observations made in the modern ocean at this latitude (*24*) and is probably related to the strong temperature control on $K_{0,1,2}$ and the relatively long (in the order of 1 year) equilibration time between $CO_{2(atmos)}$ and $PCO_{2(aq)}$ (*25*). Errors in estimating T and S result in uncertainties in calculated $PCO_{2(aq)}$ of about 10 ppm (fig. S1A) (*23*). In this calculation (Fig. 3B), TA was kept constant at 2320 μeq kg^{-1}, the present value at this site. By letting TA vary as a function of salinity, the maximum glacial-interglacial shift in $PCO_{2(aq)}$ is 70 to 80 ppm, although the amplitude of variability during glacial times is increased (fig. S1B) (*23*).

The amplitude of variability in $PCO_{2(aq)}$ on shorter time scales than glacial-interglacial changes is relatively high compared with that observed in ice records. Although the Vostok data shown here are not of particularly high resolution (more variability may be expected on shorter time scales), we may well expect atmospheric records to show less variability than their marine counterparts. This is due to the near homogeneous state of atmospheric gases compared with the highly variable nature of PCO_2 in the surface ocean.

The study suggests that glacial-interglacial changes in foraminiferal shell weight are related to changes in ambient carbonate ion concentration through time in response to changing atmospheric PCO_2. If this proves to be systematic of marine carbonate production in general, the process provides negative feedback to past changes in carbon dioxide as well as to anthropogenic carbon dioxide increases in the future. Though it is as yet unclear how precise this approach might be (secondary controls such as nutrient availability may also be important), measurements of shell weight offer the potential to determine which areas of the global ocean have the greatest control over shifts in atmospheric CO_2. A further application would be to in-

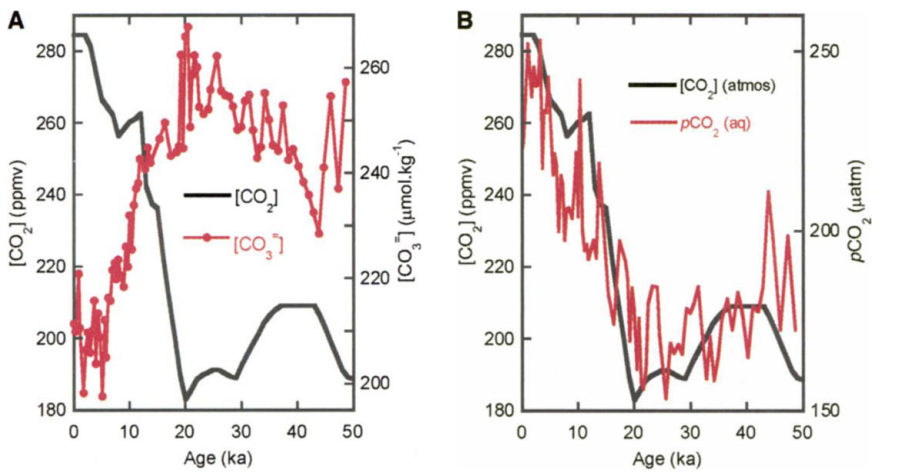

Fig. 3. (**A**) Calculated surface seawater [CO_3^{2-}] estimated from NEAP 8K together with atmospheric [CO_2] from the Vostok ice core. (**B**) Calculated surface seawater $PCO_{2(aq)}$ with Vostok atmospheric [CO_2].

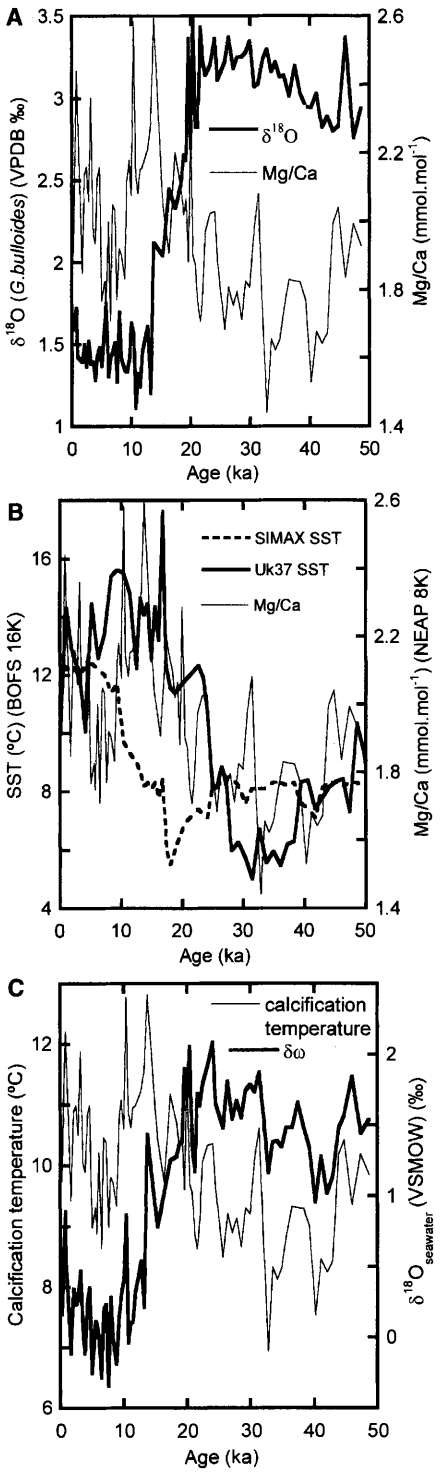

Fig. 4. (**A**) Mg/Ca and $\delta^{18}O$ for *G.bulloides* from NEAP 8K. (**B**) Mg/Ca from NEAP 8K with Faunal (SIMAX) and alkenone (Uk37) temperature estimates from nearby BOFS 16K (collected as part of the Biogeochemical Ocean Flux Study) (*36*). (**C**) Calculated calcification temperatures from Mg/Ca [Mg/Ca = $0.72 \times e^{0.1 \times T}$, where T is temperature in °C] and corresponding values of $\delta^{18}O_{seawater}$ for the same samples.

vestigate longer-term trends in $[CO_3^{2-}]$ and PCO_2. The observations made here also provide potential to refine the estimates of deep-ocean $[CO_3^{2-}]$ based on the assumption that foraminiferal shell weight is an index of dissolution (*12*). Such estimates clearly require prior knowledge of initial weight, which might be attained from a nearby shallow-core calibration or possibly by using an atmospheric PCO_2 record. It is interesting to note that the shell weights of undissolved foraminiferal calcite appear to trace surface-ocean $[CO_3^{2-}]$, whereas those of dissolved foraminiferal calcite appear to trace $[CO_3^{2-}]$ of the deep ocean.

References and Notes

1. W. S. Broecker, T. Takahashi, H. J. Simpson, T. H. Peng, *Science* **206**, 409 (1979).
2. J. A. Kleypas *et al.*, *Science* **284**, 118 (1999).
3. D. A. Wolf-Gladrow, U. Riebesell, S. Burkhardt, J. Bijma, *Tellus* **51B**, 461 (1999).
4. C. Langdon *et al.*, *Global Biogeochem. Cycles* **14**, 639 (2000).
5. U. Riebesell *et al.*, *Nature* **407**, 364 (2000).
6. F. Marubini, H. Barnett, C. Langdon, M. J. Atkinson, *Mar. Ecol. Prog. Ser.* **220**, 153 (2001).
7. I. Zondervan, R. E. Zeebe, B. Rost, U. Riebesell, *Global Biogeochem. Cycles* **15**, 507 (2001).
8. S. J. Zhong, A. Mucci, *Chem. Geol.* **78**, 283 (1989).
9. P. Zuddas, A. Mucci, *Geochim. Cosmochim. Acta* **62**, 757 (1998).
10. H. Spero, J. Bijma, D. W. Lea, B. E. Bemis, *Nature*, **390**, 497 (1997).
11. J. Bijma, H. Spero, D. W. Lea, in *Uses of Proxies in Paleoceanography: Examples from the South Atlantic*, G. Fischer, G. Wefer, Eds. (Springer-Verlag, Berlin, 1999), pp. 489–512.
12. W. Broecker, E. Clark, *Paleoceanography* **16**, 531 (2001).
13. H. Elderfield, G. Ganssen, *Nature* **405**, 442 (2000).
14. W. S. Broecker, personal communication.
15. For weight analysis, 20 to 24 individual shells were picked, with care given to ensuring the highest degree of morphological consistency. The shells were weighed using a seven-place microbalance (precision = 0.1 μg), the mean weight being taken to represent that population. Size analysis of foraminiferal tests was performed on digital photomicrographs using OPTIMAS image analysis software. Two-dimensional analysis of individual sample populations allows measurement of mean major axis length (*L*) and cross-sectional area (*A*). These values may be used to normalize the mean weight of the sample to the average size for that sieve-size fraction. In this case, normalized L = 436 μm and A = 0.113 mm^2.
16. W. Broecker, E. Clark, *Geochem. Geophys. Geosyst.* **2**, 2001GC000185 (2001).
17. ———, *Geochem. Geophys. Geosyst.* **3**, 2001GC000231 (2002).
18. D. W. Oppo, S. J. Lehman, *Science* **259**, 1148 (1993).
19. C. J. Bertram, H. Elderfield, N. J. Shackleton, J. A. Macdonald, *Paleoceanography* **10**, 563 (1995).
20. $[CO_3^{2-}]$ values were calculated from TA, TCO_2, T, P, S, $[PO_4]$, and $[SiO_4]$ taken from the North Atlantic WOCE database (*26*) using the CO2SYS program (version 01.05) (*27*). Adjustment to preindustrial values was made by recalculation via CO2SYS using preindustrial PCO_2 (= 0.8 × modern PCO_2) values. Values of $[CO_3^{2-}]$ used in the calibration were calculated for a particular sample via the temperature (*28*) for June at 30-m water depth (assumed calcification season and depth of *G. bulloides*) for the sample site.
21. The CO_2 record used here is plotted on the time scale calculated by tuning Vostok $\delta^{18}O$ to the June insolation curve at 65°N (*29*). Using this time scale allows for better correlation between ice-cores and marine records.
22. Empirical values of $K_{0,1,2}$ in terms of T and S were taken from Millero (*30*). Carbonate alkalinity, CA, $([HCO_3^-]+2[CO_3^{2-}])$ is considered equal to 96% of TA, allowing for the contributions from borate and water (plus minor others) alkalinity. The value of 96% is taken from Zeebe and Wolf-Gladrow (*31*) as a typical seawater example ($TA \approx PA$ = 2300 μmol kg^{-1}, DIC = 2000 μmol kg^{-1}, T = 25°C, S = 35).
23. Information on sampling methods, Mg/Ca analysis, temperature, and salinity calculations and $PCO_{2(aq)}$ uncertainty estimations are available at *Science* Online.
24. W. S. Broecker, T.-H. Peng, *Tracers in the Sea* (Lamont-Doherty Geolocical Observatory, Columbia University, Palisades, NY, 1982).
25. For a discussion of the response time of PCO_2 and ΣCO_2 in surface waters, see p. 153 of (*24*).
26. WOCE (World Ocean Circulation Experiment) data are available through the Carbon Dioxide Information Analysis Centre (CDIAC) Web site, at http://cdiac.esd.ornl.gov/.
27. E. Lewis, D. W. R. Wallace, Oak Ridge National Laboratory, ORNL/CDIAC-105 (1998).
28. S. Levitus, T. Boyer, *World Ocean Atlas 1994 Volume 4: Temperature*, NOAA Atlas NESDIS 4 (U.S. Department of Commerce, Washington, DC, 1994).
29. N. J. Shackleton, *Science* **289**, 1897 (2000).
30. F. J. Millero, *Geochim. Cosmochim. Acta.* **59**, 661 (1995).
31. R. E. Zeebe, D. Wolf-Gladrow, *CO_2 in Seawater: Equilibrium, Kinetics, Isotopes*. D. Halpern, Ed., Elsevier Oceanography Series (Elsevier, Amsterdam, 2001), vol. 65.
32. NEAPACC, North East Atlantic Palaeoceanography and Climate Change data (CD-ROM) (Natural Environment Research Council, Swindon, UK).
33. G. G. Bianchi, thesis, University of Cambridge (1999).
34. P. P. E. Weaver *et al.*, *Paleoceanography* **14**, 336 (1999).

35. We thank J. Bijma and Y. Rosenthal for encouraging us to consider the carbonate ion effect, W. Broecker and R. Fairbanks for very helpful discussions supported by the ARCHES program, and F. Millero and J. Bijma for comments on the manuscript. L. Booth and M. Greaves provided invaluable laboratory support. Financial support was provided by the Natural Environment Research Council and the Cambridge-MIT Institute.

Supporting Online Material

www.sciencemag.org/cgi/content/full/297/5582/833/DC1
Methods
Fig. S1
References

12 April 2002; accepted 1 July 2002

Single-Cell Gene Expression Profiling

Jeffrey M. Levsky, Shailesh M. Shenoy, Rossanna C. Pezo, Robert H. Singer*

A key goal of biology is to relate the expression of specific genes to a particular cellular phenotype. However, current assays for gene expression destroy the structural context. By combining advances in computational fluorescence microscopy with multiplex probe design, we devised technology in which the expression of many genes can be visualized simultaneously inside single cells with high spatial and temporal resolution. Analysis of 11 genes in serum-stimulated cultured cells revealed unique patterns of gene expression within individual cells. Using the nucleus as the substrate for parallel gene analysis, we provide a platform for the fusion of genomics and cell biology: "cellular genomics."

The first step in the translation of genomic sequence into physiology or pathophysiology is transcription. Transcriptional regulation has been studied almost exclusively on nucleic acids extracted from cultured cells or tissues by Northern blot (*1*), differential display (*2*), serial analysis of gene expression (SAGE) (*3*), or forms of microarray (*4, 5*). Here, we describe a complementary approach that monitors mRNA synthesis by visualizing specific sites of transcription (*6, 7*). The use of transcription sites for expression profiling allows analysis of coordinated transcription events and organization of gene expression. To achieve sensitive and specific detection of RNAs by fluorescence in situ hybridization (FISH), we used oligomer DNA probes that were each tagged with a single fluorophore at multiple sites (*8*). To detect many mRNAs simultaneously, we used combinations of these probes labeled with spectrally distinct colors (Fig. 1A) (*9*). A combinatorial approach to labeling probes (Fig. 1B) provided a large number of virtual "colors" for distinguishing many transcripts (supporting online text and table S1). Spectral "barcodes" with a minimum of two distinct fluorophores were used to increase specificity. Schemes based on color combinations have been applied to detection of entire chromosomes for cytogenetics (*10, 11*) and for analysis of subchromosomal regions of DNA (*12*). However, the targets in these genomic assays are orders of magnitude larger than transcripts and do not contain functional information.

Cell culture and preparation, fluorescence microscopy, and image acquisition were performed and images were subjected to computational analysis to detect sites of transcription (*9*). Transcription sites have a

Department of Anatomy and Structural Biology, Albert Einstein College of Medicine, 1300 Morris Park Avenue, Bronx, NY 10461, USA.

*To whom correspondence should be addressed. E-mail: rhsinger@aecom.yu.edu